



Acceleration of superparamagnetic particles with magnetic fields

R. Stange*, F. Lenk, T. Bley, E. Boschke

Institute of Food Technology and Bioprocess Engineering, TU Dresden, Dresden, Germany



ARTICLE INFO

Keywords:

Biomagnetic Separation
Electromagnetic Sample Mixer
Superparamagnetic particles
CFD
Magnetic force fields

ABSTRACT

High magnetic capture efficiency in the context of Biomagnetic Separation (BMS) using superparamagnetic particles (SMPs) requires efficient mixing and high relative velocities between cellular and other targets and SMPs. For this purpose, batch processes or microfluidic systems are commonly used. Here, we analyze the characteristics of an in-house developed batch process experimental setup, the Electromagnetic Sample Mixer (ESM) described earlier. This device uses three electromagnets to increase the relative velocity between SMPs and targets. We carry out simulations of the magnetic field in the ESM and in a simpler paradigmatic setup, and thus were able to calculate the force field acting on the SMPs and to simulate their relative velocities and fluid dynamics due to SMP movement.

In this way we were able to show that alternate charging of the magnets induces a double circular stream of SMPs in the ESM, resulting in high relative velocities of SMPs to the targets. Consequently, due to the conservation of momentum, the fluid experiences an acceleration induced by the SMPs.

We validated our simulations by microscopic observation of the SMPs in the magnetic field, using a homemade apparatus designed to accommodate a long working-distance lens. By comparing the results of modeling this paradigmatic setup with the experimental observations, we determined that the velocities of the SMPs corresponded to the results of our simulations.

1. Introduction

Biomagnetic Separation (BMS) is an established tool in laboratory and clinical applications, including for example selection and enrichment of bacteria, cells, macromolecules, etc. [1–3]. Enrichment of the target renders it more amenable to detection and analysis [4]. When this is done via BMS, extensive complexation between superparamagnetic particles (SMPs) and targets is crucial for effective separation, and reduces the amount of SMPs required. To achieve complexation, however, mixing of the solution alone is insufficient; rather, the key factor are relative velocities between SMPs and the medium during mixing.

In principle, BMS involves first complex formation of SMPs and targets, and subsequent separation of the complexes in an external magnetic field, after which the complexes are removed from the supernatant and resuspended. The success of BMS relies heavily on the first step, i.e. complex formation, and for this to occur, the collision rate between reaction partners must be high. In standard BMS protocols, little attention is paid to factors, e.g. velocities and collision rate, which would influence complex formation itself.

In conventional protocols, where samples are in the milliliter range, the first mixing step is performed in an inverting shaker [2,5]. With this

method, relative velocity between targets and SMPs arises from the sedimentation differences between SMPs and targets, the difference of velocities of two neighboring stream lines of the fluid and due to thermal diffusion of the SMPs and targets [6]. Because magnetic forces can be applied that are of larger magnitude than those forces arising from effects mentioned above, they can be used to increase the relative velocity and thus improve the efficiency of complex formation. In the application of microfluidic devices, magnetic fields are commonly used only for mixing SMPs in a fluid [7] or to change their trajectory to sort them [6,8–12].

Previously, we described an Electromagnetic Sample Mixer (ESM) built in-house which was used to accelerate SMPs via a defined magnetic fields with samples in the milliliter range as a batch process [13,14]. The aim of the current study was to characterize the efficacy of the ESM, in terms of relative velocities achieved and the resulting fluid dynamics, by implementing a model. To test the accuracy and adjust the parameters of our model, two simplified paradigmatic setups were used. The first of these served to measure the magnetic fields, and in the second, the SMPs could be directly imaged and their absolute velocities in the fluid could be measured. A comparison of the simulation data with experimentally derived data guided adjustment of the parameters, such that the behavior of the SMPs in the ESM could

* Corresponding author.

E-mail address: Robert.stange@tu-dresden.de (R. Stange).

Nomenclature

B	Magnetic induction [T]
c_s	Concentration of the SMPs [1/mL]
f	Time depending function [–]
F_{fl}	Volumetric force acting on the fluid [N/m ³]
F_m	Volumetric magnetic force [N/m ³]
f_u	Frequency of switching the charged magnets [1/s]
F_w	Volumetric drag force due to fluid resistance [N]
H	Magnetic field [A/m]
k_u	Factor for time signal [–]

t	Time [s]
t_{imp}	Impulse time [s]
r_m	Radius of the magnetic core of the SMPs [m]
r_s	Radius of the SMPs [m]
v_{abs}	Absolute velocity of SMP [m/s]
v_{fl}	Fluid velocity [m/s]
v_{rel}	Relative velocity between SMP and fluid [m/s]
x, y	Continuum spatial coordinates [m]
η	Dynamic viscosity [Pa s]
μ_r	Relative magnetic permeability [–]
μ_0	Magnetic permeability in vacuum [V s/(A m)]

be simulated and analyzed to understand mechanisms behind interaction of SMPs and targets.

2. Materials and methods

2.1. Electromagnetic Sample Mixer (ESM)

The essential element of the ESM consisted of a construction containing three customized magnetic cores. As shown in Fig. 1, the general principle used in this study remained the same as in the original device [13]: the middle of the three planes has the opposite orientation of the pole shoe geometry to the other two, giving a magnetic gradient in the reverse orientation.

The process of charging the magnets was divided into two steps. In the first, only the upper and lower magnets were charged, leading to movement of the SMPs in the direction of magnetic gradient from right to the left in Fig. 1. In the second step the middle plane of the magnets with the opposite orientation of pole shoe geometry was charged to accelerate the SMPs in the opposite direction from right to left [14].

2.2. Observation of SMP movement

For imaging SMP movement, a WF Olympus upright microscope (Olympus Deutschland GmbH, Hamburg, Germany) outfitted with a long working distance lens (1) (SLCPlanFL 40× 0.55) was used. Observations were carried out in the simplified customized setup shown in Fig. 2. In this setup, just one magnet is used to enable the observation under the microscope, which is not possible using the entire ESM apparatus.

Fig. 2 shows one magnetic core (2) of the ESM being fixed in a 3D printed holder (3). The sample (4) is situated in the pole shoe geometry on an object slide and consists of 4 parts (Fig. 3 B). Two cover slips (5, 7) with a diameter of 13 mm created a fluid chamber with a ring (6) of diameter 10 mm and a height of 2 mm to give a volume of appx. 150 μ L. Before covering the chamber with coverslip (5) the particle suspension was filled in. A spacer (8) was used to adjust the height of the sample in the magnetic field. With a DC power supply (NSP 3630,

Manson Engineering Industrial Ltd, Hong Kong) the current in the coils can be set.

Experiments to determine SMP movement were performed under a current of 400 mA in the coil. Experiments were divided into 3 phases: During the first and third phases, each lasting 5 s, the magnetic field was turned off, removing any magnetic force acting on the SMPs. The second phase was the on-phase, with a duration of 10 s. Charging of the magnet resulted in a magnetic force that acted on the SMPs and induced their acceleration. The videos were recorded at a frame rate of four pictures per second and a resolution of 1300×1030 pixel of the CCD camera (CoolSNAP fx, Pkotometrics, Tucson, USA). Pixel dimensions were 0.1858 μ m/pixel equals a recorded square of 0.23×0.18 mm².

Velocity analysis of the SMPs from image stacks exported from the software Metamorph were carried out in ImageJ (Fiji). The images were first converted to 8 bit color depth and a value of 10 was added to the intensity. With a threshold brightness intensity of 5, several SMPs tagged with black points were visible on a white background. The trajectories of the SMPs were then analyzed with the tracking algorithm Mtrack2 implemented in Fiji, with maximum velocity set to less than 200 pixels travelled between frames. The track length was set to three frames minimum. The results were exported to Excel to calculate the absolute velocities of the SMPs.

SMPs were suspended in 50 mM HEPES buffer, adjusted to pH 6.7 with 1 M KCl. The final concentration of SMPs was 5.10⁸/mL.

2.3. Magnetic field measurements

Evaluation of magnetic field simulations was performed with a customized setup, representing one electromagnet of the ESM, mounted on an experimental stand, shown in Fig. 3.

The apparatus constructed for the measurement of magnetic induction B to evaluate the magnetic field \vec{H} simulations was designed as follows: a magnetometer (1, Gaußmeter MNT 4E04 VH, Lake shore Cryotronics Westerville, Ohio, USA) is held in place with the gallows (2). To measure x and y components of B , the gallows allows insertion of the magnetometer in two different orientations orthogonal to each

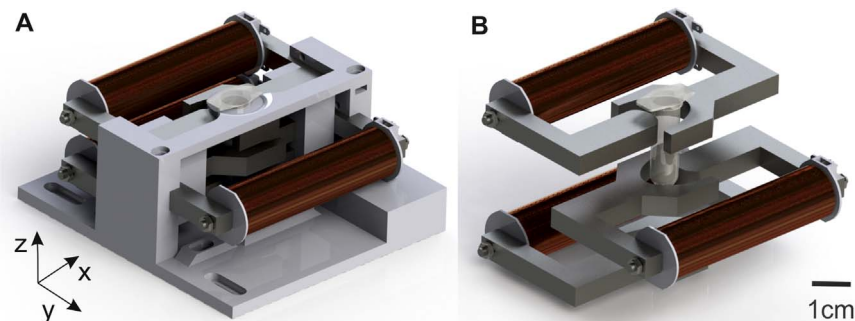


Fig. 1. CAD illustration of the ESM with three magnetic cores arranged in three planes, where the middle plane has the opposite direction of elliptical pole shoe geometry which can be seen in A: in the 3D printed holder to fix the positions of the magnetic cores, and in B: exploded view of the three planes of magnets.

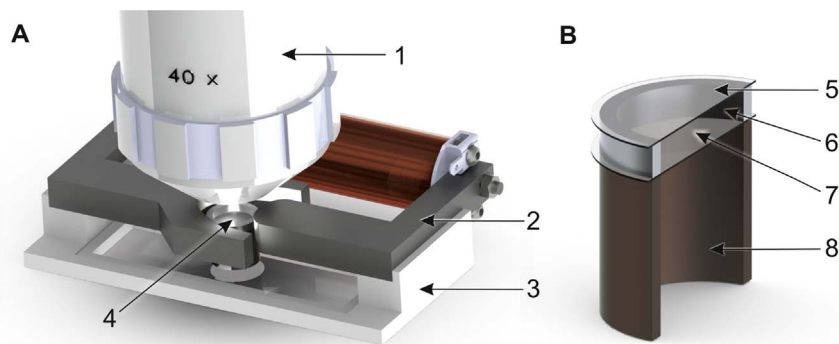


Fig. 2. CAD illustration of the setup for microscopic imaging of SMP movement. 1: long working distance lens; 2: magnetic core with coil; 3: holder; 4: fluid chamber seen in B, 5 and 7: cover slips to close the chamber 6; 8: spacer.

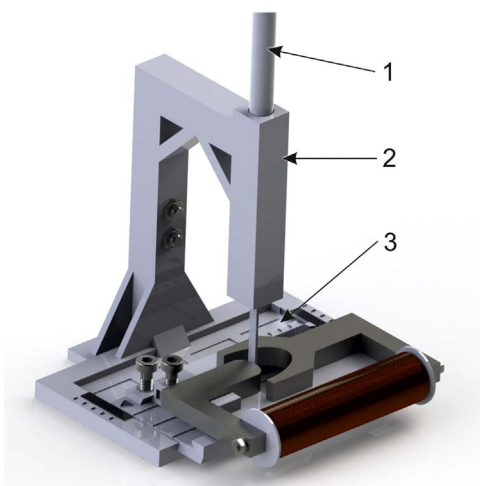


Fig. 3. CAD illustration of the setup for magnetic induction B measurements, 1: magnetometer; 2: gallows; 3: base plate with slide system.

other. The height (z -position) of the gallows and the x - y -position of the magnetometer could be adjusted with a slide system (3). All parts were 3D printed. To charge the coil, the same power supply was used as for the observation of SMP movement described in Section 2.2.

This arrangement allows the experimenter to map the air gap between the pole shoes in all three dimensions, such that the two components (x , y) of B may be measured at any given point in the 3D space defined by the sliders; further, the B itself can be modulated by inducing different currents in the coil.

2.4. SMPs used in the study

1 μm diameter SiMAG PEI SMPs (Chemicell GmbH, Berlin, Germany) with a crystalline core of maghemite coated with silicon oxide were used in our study. For potential cell applications of the BMS system, particles coated with a third layer of positively charged polyethylene imine (PEI) were obtained. The coating in principle allows binding between targets and SMPs based on electrostatic interactions. The density of the SMPs is 2250 kg/m^3 .

3. Models used for simulations

Simulations were performed with COMSOL Multiphysics. The Magnetic Fields Physics application from the AC/DC module was used to simulate the magnetic field (detailed in Section 3.1). The magnetic force acting on the SMPs (see Section 3.2), derived from the magnetic field, was used to calculate the relative velocities of the SMPs by applying our own equations in COMSOL (see Section 3.3). The simulation of fluid flow was implemented in the Laminar Flow module.

3.1. Simulation of the magnetic field

Simulations of the volumetric magnetic force \vec{F}_m acting on the magnetic core of the SMPs requires a knowledge of the values of the magnetic field \vec{H} between the pole shoe geometry. To obtain these values we used the Magnetic Field Physics application in COMSOL Multiphysics. We implemented a geometry created in SolidWorks that in turn contained a coil geometry where the diameter was calculated with a filling factor of 1, ignoring the space between the wire coils. In addition, a geometry for the airgap between the pole shoes was created to produce a finer mesh in the air gap during the numerical calculations. The following materials were assigned to the different domains of the geometry for parameter definition: The coil was assigned as copper. The holder of the coil and the surrounding air as well as the gap geometry were assigned as air with a magnetic permeability of 1. The parts of the magnetic core were assigned as soft steel, where we exchanged the HB and BH curves with the values from soft iron [15]. The equations to solve the magnetic field were based on Amperes law. The temperature for the simulation was set to 20 $^\circ\text{C}$.

A circular multi-turn coil was used to define the coil domain where the magnetic field induction is described with the magneto motive force, where the current and the number of windings determine the magnitude of the magnetic field induction. The parameters in the coil were adjusted analogously to the measurements of the magnetic induction B in order to produce comparable results (3500 windings, 900 mA, 600 mA, 200 mA).

3.2. Simulation of force acting on the SMPs

It was important to know the force acting on the magnetic core of the SMPs in order to derive the velocities of the SMPs relative to the fluid \vec{v}_{rel} . Due to the conservation of momentum, we can calculate the force acting on the fluid, which gives a velocity of the fluid \vec{v}_f during the simulation of fluid flow.

The model simulating the force acting on the SMPs \vec{F}_m , carried out in COMSOL, is based on the simulated \vec{H} applied via the magnets [16]. In Eq. (1) i is the index for the three components in the x -, y - and z -direction and μ_0 is the magnetic permeability in the vacuum.

$$\vec{F}_m = \mu_0 (\mu(|\vec{H}|) - 1) \frac{dH_i}{dx_i} \vec{H}_i \quad (1)$$

For the permeability of the magnetic cores of the SMPs $\mu(|\vec{H}|)$, which is dependent on the $|\vec{H}|$ the following fitting can be used for the maghemite core. The fitting data are based on the measurement of the manufacturer (personal information from Chemicell GmbH).

$$\mu(|\vec{H}|) = \begin{cases} 133 & |\vec{H}| < 3300 \text{ A m}^{-1} \\ 7047.7 |\vec{H}|^{-0.49} & |\vec{H}| \geq 3300 \text{ A m}^{-1} \end{cases} \quad (2)$$

The curve representing $\mu(|\vec{H}|)$, as a function of $|\vec{H}|$ fits at the $|\vec{H}|$ values attained in the magnetic core of the ESM at the used currents to induce the magnetic fields. If $|\vec{H}|$ approaches the saturation range of the magnetic material the error will increase, rendering this fitting inapplicable.

3.3. Simulation of relative velocities of the SMPs

The model to simulate \vec{v}_{rel} is based on the equilibrium of the \vec{F}_m due to the magnetic field and the fluid resistance \vec{F}_w according to Stokes law (Eq. (3)), which can be used because of the low Reynolds number. In Eq. (3), η is the viscosity of the medium which is defined as 1 mPa s. The model calculates the \vec{v}_{rel} considering no particle-particle-interactions.

$$\vec{F}_w = \frac{9}{2} \frac{\vec{v}_{rel} \eta}{r_s^2} \quad (3)$$

Two parameters of the SMPs were defined to take the magnetizable volume into account, first the radius of the whole sphere with r_s and second, the radius of the maghemite core with r_m .

$$\vec{v}_{rel} = \frac{2}{9} \frac{r_m^3 \vec{F}_m}{\eta r_s} \quad (4)$$

This approach to calculate SMP velocities was used by Häfeli et al. [17], who compared the calculated velocities with experimental data for different types of SMPs.

Eq. (4) was implemented in COMSOL to simulate the relative velocities.

3.4. Simulation of fluid movement

Simulations of the magnitude of the fluid flow associated with the acceleration of the SMPs were performed to evaluate the mixing process. It is assumed that, based on Newton's second law, the movement of SMPs also accelerates the surrounding fluid. Given the large number of SMPs in suspension, this effect of drag on the fluid should in turn influence SMP movement, which we observe microscopically. In addition to this mutual influence of the fluid dynamics and the SMP movement, another layer of complexity is introduced in the context of the whole ESM by virtue of the oscillating magnetic force fields applied. This is expected to have even more variable effects on interactions between the SMPs and their surrounding that come about as a result of double circular streaming of the fluid.

The force acting on the SMPs and transferred to the fluid due to the conservation of momentum [18] can be described with the volumetric force \vec{F}_{fl} . Eq. (5) takes the volume fraction of the magnetic cores of the SMPs into account and relates it to \vec{F}_m where c_s is the effective concentration of the SMPs.

$$\vec{F}_{fl} = \vec{F}_m \frac{4}{3} \pi r_m^3 c_s \quad (5)$$

This model of force acting on the fluid includes the following assumptions:

- The friction energy transferred to the fluid can be ignored.
- The SMPs are homogeneously dispersed in the fluid throughout the experiment.

The model was also used by Warnke who described the method to simulate the fluid movement due to particle acceleration. He investigated behavior of the separation of the particles with a static external magnetic field over time [18].

For the implementation of this model of fluid flow a modified SolidWorks model was used where a geometry of the fluid was

constructed to create a domain of the fluid in COMSOL. At first \vec{H} was simulated as described in Section 3.1. To derive \vec{H} in COMSOL it has to be transformed with a PDE-physic operation. \vec{F}_m was calculated using Eq. (1). r_m , r_s and c_s were defined as global parameters. $\mu(|\vec{H}|)$ (Eq. (2)) was implemented as an analytical function. For the fluid dynamic the Laminar Flow Physic module in COMSOL was used. In this module, a volumetric force acting on the fluid was defined using Eq. (3). In the setup of SMP observation depicted in Fig. 2, this force was constant throughout the simulation.

The implementation of the model of fluid movement for the whole ESM with its three magnets is in principle analogous to the paradigmatic situation of SMP observation in the single-magnet setup. But \vec{H} and \vec{F}_m must be simulated twice due to the charging protocol, involving oscillating charging of the upper and lower magnet (process step 1), and then the middle magnet (process step 2). Due to the different force fields, a time dependency of \vec{F}_{fl} in the laminar flow module must be introduced. For this reason in Eqs. (6) and (7) a sine function is coupled with a condition taking into account an impulse time t_{imp} which is the duration between the two steps like it is presented in Fig. 4. This t_{imp} is a feature of the ESM, on which future studies will focus.

$$f_1(t) = \begin{cases} 1, & \sin(\pi f_u t) > k_u \\ 0, & \sin(\pi f_u t) \leq k_u \end{cases} \quad (6)$$

$$f_2(t) = \begin{cases} 1, & \sin\left(\pi f_u \left(t + \frac{1}{f_u}\right)\right) > k_u \\ 0, & \sin\left(\pi f_u \left(t + \frac{1}{f_u}\right)\right) \leq k_u \end{cases} \quad (7)$$

In Eqs. (6) and (7) f_u is the frequency of oscillation in the switching between the magnets and k_u is a parameter to include t_{imp} which defines the duration of charging of the magnet and creates a ratio between the on and off time in one oscillating step.

$$k_u = \sin\left(\frac{1}{2} \pi f_u t_{imp}\right) \quad (8)$$

With these time dependent terms ($f_1(t)$, $f_2(t)$) the final \vec{F}_{fl} for the ESM can be calculated by the following equation:

$$\vec{F}_{fl} = (f_1(t) \vec{F}_{m1} + f_2(t) \vec{F}_{m2}) \frac{4}{3} \pi r_s^3 c_s \quad (9)$$

A time dependent study was chosen to solve the model in COMSOL using this expression.

4. Results

In a previous study, an ESM was used to accelerate SPMS in a

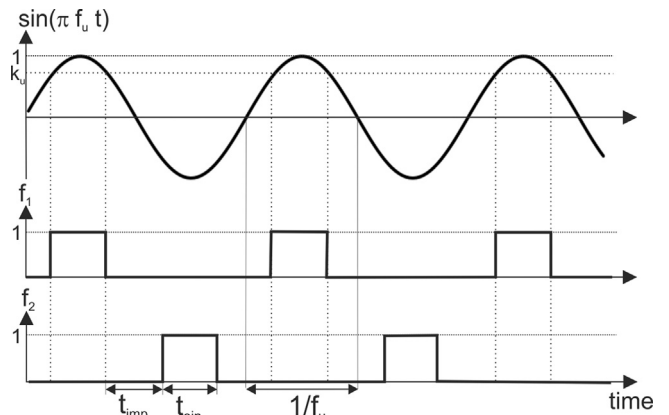


Fig. 4. Illustration of the behavior of the parameters from Eqs. (6)–(8).

medium subjected to variable magnetic fields, which allowed the mixing process to be directed in a defined manner.

An innovation in the design presented here differs from the previously published device [13] in the material of the magnetic cores as well as in the coil area. In both designs of the ESM, the elliptical geometry of the pole shoes, which constitute the heart of the device, produces a smooth gradient in the magnetic field, which results in a directed acceleration of SMPs. The current setup (shown in Fig. 1A) differs from the original design in that the coil cylinders are larger in cross section to decrease magnetic saturation effects. In addition, a different material, soft iron, was used, and the number of windings was reduced in order to preserve the same coil diameter. These improvements gave an increased magnitude of magnetic field in the pole shoe geometry.

Through the oscillation of the two charging steps in the ESM, a double circular streaming of the SMPs is expected to occur, together with streaming of the fluid due to the conservation of momentum. However, SMP movement in the ESM is difficult to visualize experimentally due to the height of the sample container and the surrounding magnetic cores.

In order to approach this problem, we created two simplified paradigmatic setups, one to analyze the magnetic field, and one to visualize SMP movement microscopically.

4.1. Magnetic field measurements and simulations in a paradigmatic setup

The force exerted on the SMPs by the electromagnets provided the basis for our estimation of the \vec{v}_{rel} of the SMPs in solution, and the force acting on the fluid. To calculate \vec{F}_m , \vec{H} in all three dimension is needed. Fig. 5A shows $|\vec{B}|$ between the pole shoes of the magnetic cores with a current of 400 mA which was used in the following simulations and all subsequent experiments on actual SMP movement. The maximum of $|\vec{B}|$ is situated at the smaller core due to the smallest air gap between the two geometries where the main flux passes. To evaluate the simulations of the magnetic field, the x-component of B was measured with the simplified paradigmatic setup described in Section 2.3 and compared to the simulations (Fig. 5B). The y-axis of the graph depicts the magnetic flux measured in the simulation, and from the experimental data, at different points x along the line given by the symmetric plane that bisects the elliptical geometry of the pole shoes in Fig. 5A. Interestingly, we note a saturation effect of the magnetic core as evidenced by the fact that the magnetic induction does not increase linearly with the current. The comparison between the simulation and the experimental data shows a good correlation.

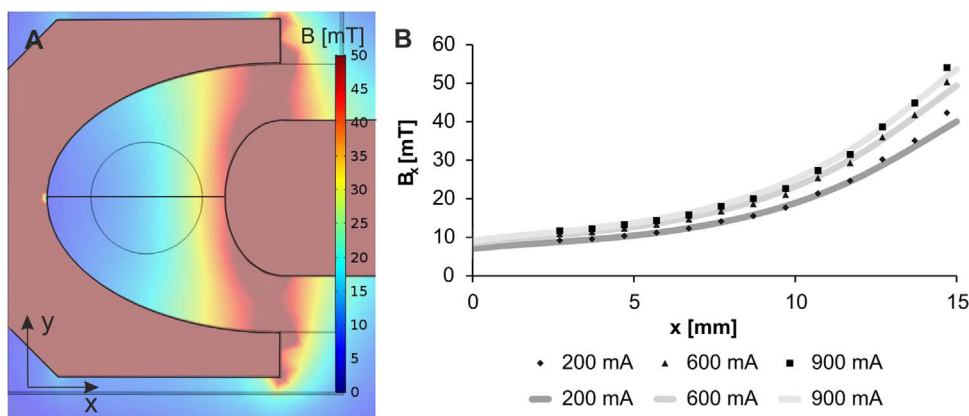


Fig. 5. A: top view of the magnetic field simulation in the pole shoe geometry of one magnet with 400 mA. The color bar shows the strength of the magnetic field from 0 (dark blue) to 5.10^4 A/m (red) B: comparison of experimental data (boxes, triangles) and simulations of the magnetic induction (lines) in the symmetry plane of pole shoe geometry with different currents in the coil to induce the magnetic fields. (For interpretation of the references to color in this figure legend, the reader is referred to the web version of this article.)

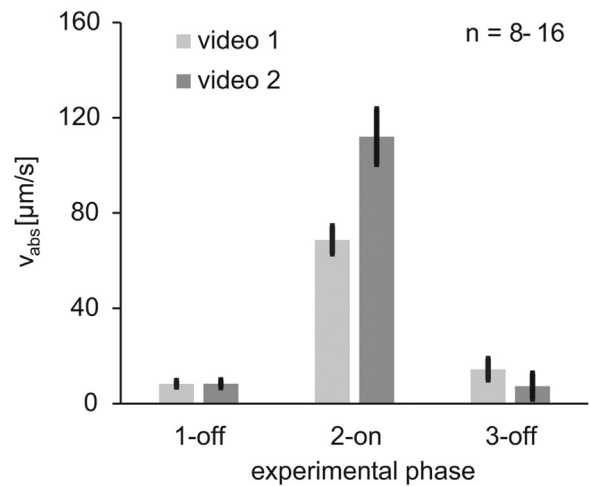


Fig. 6. Average velocities of tracked SMPs in the different phases, where the magnet was either charging (for a duration of 10 s) or off (a duration each of 5 s), from two videos obtained with the setup shown in Fig. 2 with a current of 400 mA and an initial particle concentration of $c_s=5 \cdot 10^8$ /mL.

4.2. SMP movement in the paradigmatic setup

Several different phenomena were observed during the experimental visualization of SMP movement in the magnetic field. First, the SMPs, which have a higher density compared to the medium ($2250\text{kg}/\text{m}^3$ vs. $1000\text{kg}/\text{m}^3$), sedimented at the bottom of the sample chamber, leading to a lower effective SMP concentration, c_s . As a result, the fraction of magnetizable volume able to accelerate the fluid also decreased. Another factor that compromised the dispersion, and therefore c_s in the fluid was the attachment of SMPs to the wall near the maximum region of the magnetic field. Furthermore, a thermal flow in the fluid due to heat from the light source of the microscope was visible, leading to a circular flow traversing the fluid chamber between the two cover slips shown in Fig. 2B. The center in the middle plane, where the velocity of thermal flow was zero, was used to focus the SMPs for microscopic visualization.

Fig. 6 shows the average velocities of tracked SMPs during the different phases (on or off) of two experiments (dark and light gray). The results show that the velocities of the SMPs during the charging (2-on) phase is much higher than in the off phases (1-, 3-off). The difference between the two velocities obtained in the on-phase from the two videos could be a consequence of loss of effective c_s due to the factors discussed above, namely sedimentation and accumulation on the wall. However, the large difference between the on and off phases

Table 1
Simulation results of the SMP velocities with different r_m and c_s .

Changed parameters		Simulation results		
Radius of magnetic core r_m [μm]	Concentration of SMPs c_s [1/mL]	Relative velocity $ \vec{v}_{rel} $ [$\mu\text{m/s}$]	Fluid velocity $ \vec{v}_f $ [$\mu\text{m/s}$]	Absolute velocity $ \vec{v}_{abs} $ [$\mu\text{m/s}$]
0.2	1.10^9	5,6	2950	2956
0.2	5.10^8	5,6	1485	1491
0.2	1.10^8	5,6	299	305
0.2	5.10^7	5,6	150	156
0.15	1.10^9	2,3	1254	1256
0.15	5.10^8	2,3	630	632
0.15	1.10^8	2,3	126	128
0.15	5.10^7	2,3	63	65

show a significant effect on absolute SMP velocities due to the magnetic field of our customized magnet. In principle, a higher fluid velocity could be achieved if more of the SMPs were mobilized, and not attached at the wall, as would be the case in the entire ESM setup. We note that the error bars of the velocities in the on-phase are relatively small, indicating a standard deviation of around 10%. Since we saw agglomerates, whose relative velocities \vec{v}_{rel} should be much higher due to their higher magnetizable volume, the variability of the absolute velocities \vec{v}_{abs} , depend on the contribution from \vec{v}_{rel} to \vec{v}_{abs} . We assume that the small errors we obtained can be attributed to a low \vec{v}_{rel} component and a higher component of low-variability \vec{v}_{fl} during the tracking of the SMPs.

Simulations of \vec{v}_{rel} and \vec{v}_{fl} were performed to evaluate the \vec{v}_{rel} between the SMPs and the fluid due to \vec{F}_m . In the simulations, two parameters (r_m and c_s) were varied to compare the simulation results with the velocities measured during the actual experiments. The concentration of SMPs diminishes compared to the initial sample due to the sedimentation and accumulation on the floor or wall of the sample chamber, as mentioned above. Table 1 shows the results of this investigation where the values were taken from the center of the fluid volume.

The results of the simulations show an influence only of the r_m s, but not c_s , on the \vec{v}_{rel} s, calculated from Eq. (4). In the model for the simulation, we assume that particle-particle-interactions do not contribute to \vec{v}_{rel} , and are therefore not considered in Eq. (4). The values of \vec{v}_{fl} , in contrast, do change significantly with both r_m and c_s . The comparison of \vec{v}_{rel} and \vec{v}_{fl} shows a higher component of \vec{v}_{fl} to the \vec{v}_{abs} than \vec{v}_{rel} .

The best match to the experimental data is reached with $r_m=0.15 \mu\text{m}$ and for video 1 at $c_s=5 \cdot 10^7/\text{mL}$ and for video 2 at $c_s=1 \cdot 10^8/\text{mL}$, suggesting that the effective concentration of SMPs in the fluid is

around 10% and 20% of the initial concentration of $c_s=5 \cdot 10^8/\text{mL}$ for video 1 and video 2, respectively. If we assume that c_s is even lower than 10–20% of the initial concentration, this would allow for an $r_m=0.2 \mu\text{m}$ and effective $c_s=5 \cdot 10^7/\text{mL}$ to reproduce the results of video 2. However, this would require a much lower concentration for video 1. The results of the (fitting) described above demonstrate that we are able to obtain results with our simulations that match experimental observations.

We next wanted to assess the behavior of the SMPs in simulations throughout the x-y extent of the circular fluid chamber. Fig. 7A shows the simulation results of \vec{v}_{rel} , where the magnitude and direction of the vectors in the horizontal plane of the fluid chamber for $r_m=0.15 \mu\text{m}$ are shown in a top view. Also the boundaries of the magnetic core geometry can be seen. Left is the bigger elliptical geometry of the pol shoes and on the right hand side is the small geometry with the magnetic maximum. A continual increase from the left to the right is presented, as was shown with $|\vec{B}|$ (Fig. 5) where the maximum was reached at the right of the graph. The values of \vec{v}_{rel} presented in Fig. 7 are proportional to \vec{F}_m , because of the Eq. (4) depends only on r_m^3 .

Fig. 7B shows the values of \vec{v}_{rel} along the line of symmetry of the fluid chamber and compares the behavior of the two values of r_m used in the simulations shown in Table 1. As it is presented, the value of the \vec{v}_{rel} of the SMPs due to \vec{F}_m depends strongly on r_m . With $r_m=0.2 \mu\text{m}$ values, relative velocities up to $|\vec{v}_{rel}|=20 \mu\text{m/s}$ are reached. A radius of $r_m=0.15 \mu\text{m}$ leads to a relative velocity of around $|\vec{v}_{rel}|=9 \mu\text{m/s}$. At the minimum of $|\vec{H}|$, \vec{v}_{rel} of both simulations are in the range 1–3 $\mu\text{m/s}$. Compared to the sedimentation velocity of the SMPs of around 0.7 $\mu\text{m/s}$ [2], the relative velocities achieved with our method are much higher for both radii.

Fig. 8A shows the \vec{v}_{fl} magnitude and direction vectors obtained in the simulation of a hypothetical sample having $r_m=0.15 \mu\text{m}$ and $c_s=1 \cdot 10^8/\text{mL}$. Here, the maximum \vec{v}_{fl} magnitude occurs along the centerline but slows at the maximum point of \vec{F}_m due to the congestion of fluid at the wall. Due to the continuity equation, a back flow occurs in an incompressible fluid resulting in movement of the whole fluid in two circles of opposing direction, as the vectors in Fig. 8A show. This results in two points having very low \vec{v}_{fl} (blue spots above and below the centerline), occurring next to the maximum. We note further that the \vec{v}_{fl} is very low in the area at the left wall. Presumably due to the small \vec{v}_{fl} and the maximum \vec{F}_m found at the right wall, separated SMPs would not be able to be remobilized up from the fluid. These results correspond with the simulations of Warnke [18].

4.3. Simulation of SMP movement in the ESM

Experimental visualization of SMP movement in the ESM itself is difficult with available imaging tools, due to physical obstruction by the

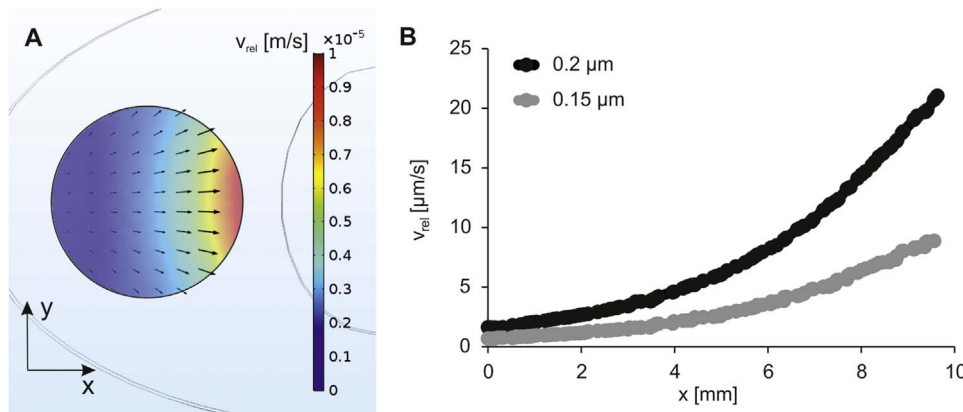


Fig. 7. A: top view of a simulation of the relative velocities of the SMPs in the setup of SMP observation with $r_m=0.15 \mu\text{m}$. B: a comparison of simulation results of relative velocity with two different radii of magnetic core of the SMPs along the line of symmetry of the fluid chamber.

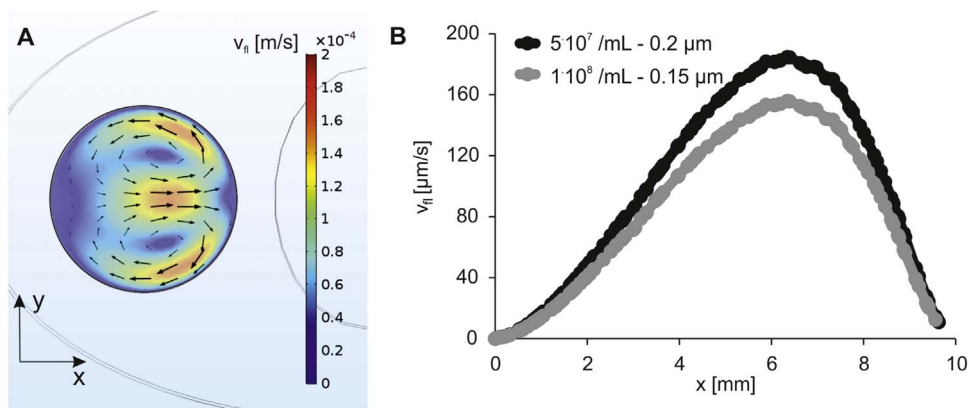


Fig. 8. A: top view of the simulation of the magnitude of fluid velocity with an SMP concentration of $c_s=1 \cdot 10^8$ /mL and a radius of $r_m=0.15 \mu\text{m}$, B: Comparison of simulations of fluid velocity using two combinations of c_s and r_m , along the line of symmetry in the fluid chamber. (For interpretation of the references to color in this figure legend, the reader is referred to the web version of this article.)

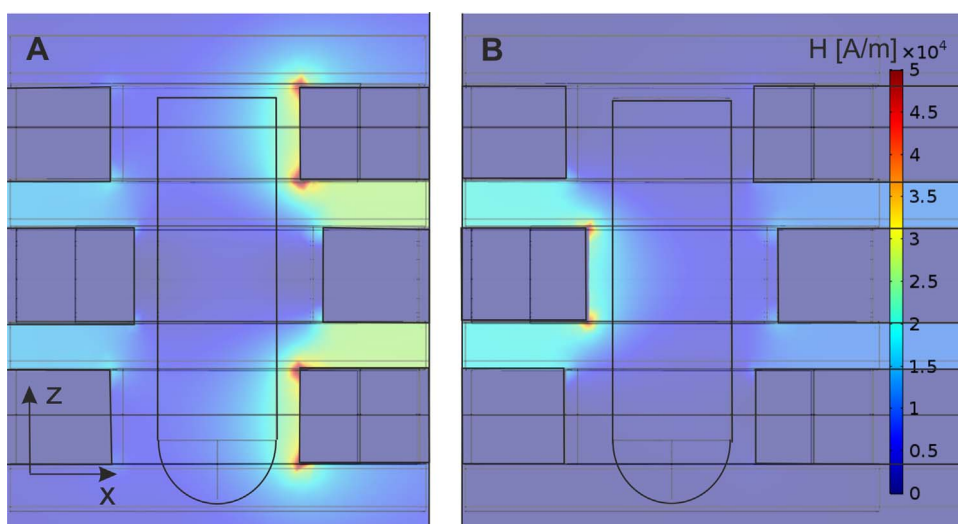


Fig. 9. Side view of the magnetic fields obtained from the simulation in the ESM with three magnetic planes and a current of 400 mA. A: process step 1 (upper and lower magnets are charged) with two coils. B: process step 2 (middle magnet is charged) with one coil.

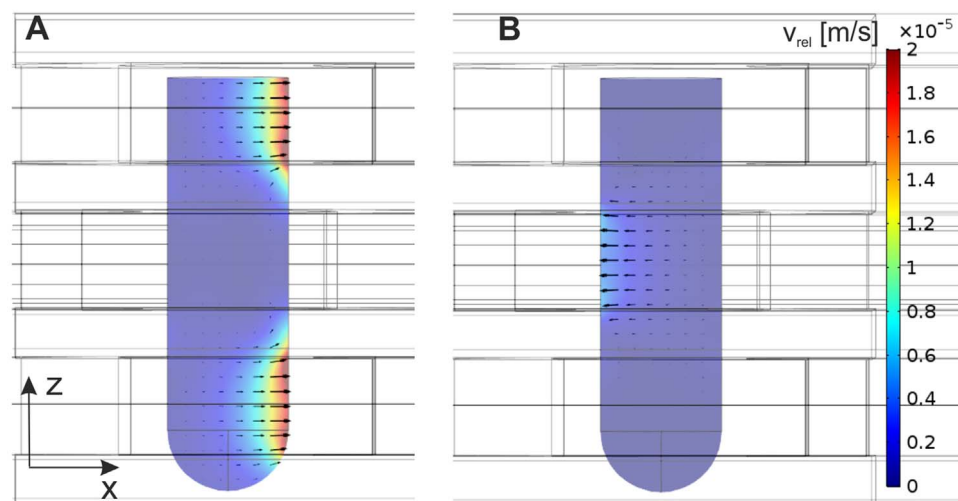


Fig. 10. Side view of relative velocities obtained from the simulations in the ESM with the three magnetic planes. A: process step 1. B: process step 2. (For interpretation of the references to color in this figure, the reader is referred to the web version of this article.)

surrounding magnetic cores and the height of the sample container. To get around this problem, simulations in the whole ESM were performed, and described below. To do this, we applied the results obtained with the paradigmatic setup, wherein SMP movement was

simulated using a fitting of the radius of magnetic core r_m to match the experimental values. The results are used to characterize the efficacy of the ESM in BMS.

The initial values were set to an SMP concentration $c_s=5 \cdot 10^8$ /mL

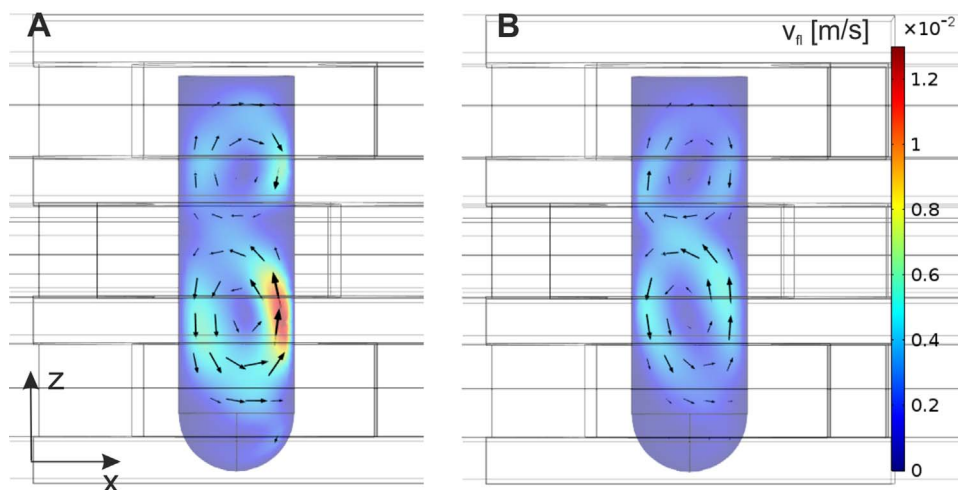


Fig. 11. Side view of fluid velocities obtained in the simulation in the ESM with the three magnetic planes. A: process step 1. B: process step 2. (For interpretation of the references to color in this figure, the reader is referred to the web version of this article.)

and a radius $r_m=0.15 \mu\text{m}$.

The simulation of the magnetic field in the ESM was analogous to the simulations of the SMP movement in the paradigmatic observation setup shown in Fig. 2A, but in this case the two process steps required simulations using two magnetic fields.

Fig. 9 shows the magnetic fields for these two steps (A: upper and lower magnets are charged, B: middle magnet is charged). The maxima of the magnetic fields occur in both illustrations at the small pole shoes, as expected in Section 2.1. Additionally, the magnetic fields in Fig. 9A are higher due to the presence of two coils inducing a higher magneto motive force.

The resulting \vec{v}_{rel} from the \vec{F}_m induced by the \vec{H} under the conditions presented in Fig. 9 is shown in Fig. 10. Here, the high relative velocities occur near to the small pole shoe geometry as in the paradigmatic test setup shown in Fig. 7. Values in the range of $|\vec{v}_{rel}|=10 - 15 \mu\text{m/s}$ are reached for process step 1 and $|\vec{v}_{rel}|=3 - 5 \mu\text{m/s}$ at process step 2, shown in panels A and B of Fig. 10. This result indicates that \vec{v}_{rel} obtained in step 1 is smaller than in the paradigmatic experimental setup ($|\vec{v}_{rel}|=9 \mu\text{m/s}$) where actual SMP movement could be observed. An explanation for this discrepancy is that the magnetic flux in the ESM setup is able to flow through the upper and lower magnetic cores instead of being confined to a single magnetic core. This could explain the decreased \vec{v}_{rel} in the middle plane of the ESM. Further, in some areas of the sample the relative velocity is lower than $1 \mu\text{m/s}$, which approaches the sedimentation velocity.

The resulting \vec{v}_f under the given conditions in the ESM are presented in Fig. 11. Due to the higher magnetic fields in step 1 than in step 2, the fluid velocity increases accordingly in step 1. As shown, the fluid indeed moves in a double circular shape as speculated in Section 4. The maxima of the fluid velocities were reached at the edges of the magnetic cores, coincident with the maxima of the magnetic fields. The maximum values of fluid velocities were up to $|\vec{v}_f| \approx 10 \text{ mm/s}$ in step 1 and up to $|\vec{v}_f| \approx 5 \text{ mm/s}$ in step 2.

The simulation of \vec{v}_{rel} that was carried out here is likely to be an accurate representation of the situation that occurs at the onset of a given experiment with the ESM. However, in reality over time particle-particle-interactions are expected to play an increasing role in the overall dynamics of the system, depending on the magnitude of the magnetic field, particle size, charge, viscosity of the medium, etc. In actual observations, two factors affect process dynamics: chain like agglomerates of SMPs may form [19,20], which will affect c_s and \vec{v}_{rel} due to a larger magnetizable volume; secondly, separation and attachment of SMPs at the wall of the sample container may also occur [18], also lowering c_s , and lowering the efficiency of BMS. These effects will be the subject of further studies.

5. Conclusions

The main aim of the study presented here was to simulate the superparamagnetic particle SMP and fluid movement in an oscillating electromagnetic field of an Electromagnetic Sample Mixer ESM developed in house.

We were able to simulate magnetic fields, as well as SMP movement and fluid dynamics in the ESM, as well as in two simpler, paradigmatic setups containing only one magnet. The simpler systems served as directly observable setups to establish and validate simulated conditions like the magnetic fields and the absolute velocity of the SMPs.

The results of magnetic field measurements show a good correlation between simulation and experimental data.

Our evaluation of the model applied in the study, is based on microscopic imaging of absolute SMP velocities in a second simplified setup with one magnet made in house. Using simulations in COMSOL, the parameters (i.e. the radius of the magnetic core of the SMP and the effect of concentration of SMPs) of the simulation were adjusted and set to match the experimental data. A lowered estimate of concentration of SMPs than initially provided was required, presumably due to the sedimentation, agglomeration and attachment of the SMPs to the wall of the fluid chamber at the magnetic field maximum. The best-fit radius of magnetic core of an SMP was used for the simulations in the ESM, in which we optimized the magnetic core and coil for this study. Additionally, the behavior of the fluid in the chamber could be seen in simulations, where a double circular movement in the horizontal plane occurred. Additionally, the simulations show a significant influence of the SMP concentration on fluid velocity.

In our simulation of the dynamics in the ESM, we determined that the peak relative velocities of the SMPs to the fluid were much higher than the sedimentation velocity. Furthermore this simulation was able to prove in this study that the hypothesized double circular streaming behavior of the fluid actually occurs, and that this is due to SMP movement.

Acknowledgement

The authors gratefully acknowledge financial support from the German Federal Ministry for Economic Affairs and Energy (BMWi), project ‘‘Optimization of Biomagnetic Separation with variable magnetic fields.’’ (KF 2049815CR3). The authors have declared no conflict of interest.

References

- [1] L. Borlido, A.M. Azevedo, A.C.A. Roque, M.R. Aires-Barros, Magnetic separations in biotechnology, *Biotechnol. Adv.* 31 (8) (2013) 1374–1385.
- [2] S. Deponte, J. Steingroewer, C. Löser, E. Boschke, T. Bley, Biomagnetic separation of *Escherichia coli* by use of anion-exchange beads: measurement and modeling of the kinetics of cell-bead interactions, *Anal. Bioanal. Chem.* 379 (3) (2004) 419–426.
- [3] Q. Chen, et al., A sensitive impedance biosensor based on immunomagnetic separation and urease catalysis for rapid detection of *Listeria monocytogenes* using an immobilization-free interdigitated array microelectrode, *Biosens. Bioelectron.* 74 (2015) 504–511.
- [4] J. Schemberg, A. Grodrian, R. Römer, G. Gastrock, K. Lemke, Online optical detection of food contaminants in microdroplets, *Eng. Life Sci.* 9 (5) (2009) 391–397.
- [5] J. Steingroewer, T. Bley, C. Bergemann, E. Boschke, Biomagnetic separation of *Salmonella Typhimurium* with high affine and specific ligand peptides isolated by phage display technique, *J. Magn. Magn. Mater.* 311 (1) (2007) 295–299.
- [6] T. Baier, S. Mohanty, K.S. Drese, F. Rampf, J. Kim, F. Schönfeld, Modelling immunomagnetic cell capture in CFD, *Microfluidic Nanofluidics* 7 (2) (2009) 205–216.
- [7] H. Suzuki, C.-M. Ho, N. Kasagi, A chaotic mixer for magnetic bead- based micro cell sorter, *J. Microelectromech. Syst* 13 (5) (2004) 779–790.
- [8] J.J. Chalmers, M. Zborowski, L. Sun, L. Moore, Flow through, immunomagnetic cell separation, *Biotechnol. Prog.* 14 (1) (1998) 141–148.
- [9] N. Pamme, On-chip bioanalysis with magnetic particles, *Curr. Opin. Chem. Biol.* 16 (3–4) (2012) 436–443.
- [10] S. Dutz, M.E. Hayden, A. Schaap, B. Stoeber, U.O. Häfeli, A microfluidic spiral for size-dependent fractionation of magnetic microspheres, *J. Magn. Magn. Mater.* 324 (22) (2012) 3791–3798.
- [11] L.R. Moore, M. Zborowski, L. Sun, J.J. Chalmers, Lymphocyte fractionation using immunomagnetic colloid and a dipole magnet flow cell sorter, *J. Biochem. Biophys. Methods* 37 (1–2) (1998) 11–33.
- [12] G. Gastrock, J. Schemberg, T. Förster, A. Grodrian, K. Lemke, B. Cahill, Markierung einzelner Zellen und deren Separation aus Zellgemischen, DE 10 2011 088 741 .5, 15-Dec-2011.
- [13] R. Stange, F. Lenk, K. Eckert, S. Lenk, T. Bley, E. Boschke, A new method for mixing of suspended superparamagnetic beads using variable electromagnetic fields, *Eng. Life Sci.* 15 (7) (2015) 727–732.
- [14] F. Lenk, R. Stange, E. Boschke, T. Bley, Vorrichtung sowie Verfahren zur Steigerung der Anbindungseffizienz von zur Bindung befähigten Zielstrukturen, DE 102013009773.8, 05-Jun-2013.
- [15] Properties of soft magnetic materials. [Online]. Available: (<http://www.fieldp.com/magneticproperties.html>). (Accessed 27-Jun-2016).
- [16] E.P. Furlani, Magnetophoretic separation of blood cells at the microscale, *J. Phys. D: Appl. Phys.* 40 (5) (2007) 1313–1319.
- [17] U.O. Häfeli, M.A. Lobedann, J. Steingroewer, L.R. Moore, J. Riffle, Optical method for measurement of magnetophoretic mobility of individual magnetic microspheres in defined magnetic field, *J. Magn. Magn. Mater.* 293 (1) (2005) 224–239.
- [18] K.C. Warnke, Finite-element modeling of the separation of magnetic microparticles in fluid, *IEEE Trans. Magn.* 39 (3) (2003) 1771–1777.
- [19] N. Wise, T. Grob, K. Morten, I. Thompson, S. Sheard, Magnetophoretic velocities of superparamagnetic particles, agglomerates and complexes, *J. Magn. Magn. Mater.* 384 (2015) 328–334.
- [20] J. Ku, H. Chen, K. He, Q. Yan, Simulation and observation of magnetic mineral particles aggregating into chains in a uniform magnetic field, *Miner. Eng.* 79 (2015) 10–16.